Form Approved
OMB No. 0704-0188

Is estimated to average 1 hour per response, including the time for reviewing instructions, searching existing data sources,
ating and reviewing the collection of information. Send comments regarding this burden estimate or any other aspect of
iducing this burden, to Washington Headquarters Services, Directorate for Information Operations and Reports, 1215 Jefferson
nd to the Office of Management and Budget, Paperwork Reduction Project (0704-0188), Washington, DC 20503.

## AD-A218 542

| Report Date. | 3. Report Type and Dates Covered. |
|---|---|
| ept. 15, 1989 | Journal Article |

**4. Title and Subtitle.**

Hurricane-Generated Currents On The Outer Continental Shelf
2. Model Sensitivity Studies

**6. Author(s).**

Cortis Cooper and J. Dana Thompson

**5. Funding Numbers.**

Program Element No. 62435N

Project No. 35G84

Task No. 2

Accession No. DN256002

**7. Performing Organization Name(s) and Address(es).**
Conoco Production Eng. & Research
Ponca City, Oklahoma

Naval Ocean Research and Development Activity   Code 323
SSC, MS 39529-5004

**8. Performing Organization Report Number.**

JA 323:031:89

**9. Sponsoring/Monitoring Agency Name(s) and Address(es).**
Office of Naval Technology
800 N. Quincy St.
Arlington, Va 22217

**10. Sponsoring/Monitoring Agency Report Number.**

**11. Supplementary Notes.**

**12a. Distribution/Availability Statement.**

Approved for public release; Distribution is unlimited.

**12b. Distribution Code.**

**13. Abstract** *(Maximum 200 words).*

**14. Subject Terms.**

Hurricanes, Coastal Currents, Numerical Modelling, Gulf of Mexico

**15. Number of Pages.**
15

**16. Price Code.**

| 17. Security Classification of Report. | 18. Security Classification of This Page. | 19. Security Classification of Abstract. | 20. Limitation of Abstract. |
|---|---|---|---|
| Unclassified | Unclassified | Unclassified | |

# Hurricane-Generated Currents on the Outer Continental Shelf
## 2. Model Sensitivity Studies

CORTIS COOPER[1]

*Conoco Production Engineering and Research, Ponca City, Oklahoma*

J. DANA THOMPSON

*Naval Ocean Research and Development Activity, Stennis Space Center, Mississippi*

A numerical model described and verified in part 1 of this two-part series (Cooper and Thompson, this issue) is applied to study the sensitivity of hurricane-generated currents on the outer shelf and slope. Numerical experiments are performed in a simple basin with a straight shelf. The sensitivity of the response to changes in storm parameters, direction of storm approach, and topography is quantified. Response is measured in terms of the mixed-layer velocity and depth at sites along the storm track. Results reveal the most important factors are (in decreasing order) wind speed, storm translation speed, direction of storm approach, asymmetry in the wind field, entrainment parameterization, and advection at slower storm translation speeds. Response is largely insensitive (less than 10%) to radius of maximum wind, shelf and slope configuration, bottom friction, atmospheric pressure gradients, and further reductions in the model grid size. For a storm approaching cross shelf, the response is primarily baroclinic (greater than 90%) and only weakly dependent (less than 10%) on the water depth at the site.

## 1. INTRODUCTION

This work represents the second part of a two-part series focusing on currents generated by hurricanes. A numerical model is the main tool used in the study, and it is described and compared with observations in part 1 [*Cooper and Thompson*, this issue] (henceforth referred to as CT). The emphasis of this work is on the outer continental shelf and slope on time scales of less than one inertial period (IP) after storm passage.

As described by CT, the numerical model uses a layered, explicit finite difference formulation based on the nonlinear primitive equations including thermodynamics, and bottom topography. In essence, the model is a logical extension of *Price*'s [1981] model to include the barotropic mode, topography, and lateral boundary influences.

CT show comparisons between the model and current measurements from three historical storms: Eloise, Frederic, and Allen. In the mixed layer, the model typically reproduces better than 80% of the observed variance with correlation coefficients of greater than 0.8. In the bottom layer, the correlation decreases, although the predicted variance still compares well. The discrepancies are probably due to unresolved local topography and nonstorm-forced mesoscale motions (e.g., warm rings).

CT also give a brief overview of the previous measurements and modeling of hurricane-driven currents. Their review reveals that little work has been done on the outer shelf and slope, and they formulate some basic questions which remain unresolved for this region: (1) What is the relative importance of horizontal gradients to mixed-layer response? (2) How does the response depend upon transla-

tion speed, size, intensity, and angle of approach of the hurricane? (3) Is there substantial nonlinear interaction between vertical modes in the presence of topography? (4) How is the response affected by the cross-shelf dimensions of the shelf and slope? (5) How is each of the above affected by local water depth? (6) What is the nature of the free wave response? (7) Where does the transition occur between primarily shallow shelf and primarily deep ocean?

Although CT gain some insight into these questions (most notably, item 6), their major purpose is to describe and verify the model. This limitation in the paper is justified because of the difficulty of resolving the questions using historical data complicated by various nonstorm effects.

It is the goal of this paper to thoroughly address most of these questions. The underlying philosophy is to remove the complexity inherent in the historical data and examine a "base" case which is simple enough to be comprehensible yet remain realistic. A thorough review of the response for this case is described in section 2. Section 3 examines the sensitivity of the base case to changes in parameters. These parameters fall into three broad categories: model formulation, storm parameters, and topography. Specifics are listed in Table 1. Section 4 summarizes the results and explicitly answers the questions posed above.

## 2. BASE CASE

### 2.1. Bathymetry and Initial Conditions

Table 2 summarizes the input parameters for the base case. The basin was started from rest with the density profile from *Price* [1981] (henceforth referred to as PR). This is typical of the eastern deepwater Gulf of Mexico during the late summer months. The model included all pressure terms except atmospheric.

A rectangular basin with a straight shelf was used as shown in Figure 1. It consisted of 20-km square elements

---

[1]Now at Coastal Leasing, Cambridge, Massachusetts.

90 02 26 116

TABLE 1. Summary of Parameters Which Were Varied, Shown in Three Basic Categories

| Category | Parameter |
| --- | --- |
| Storm parameters | radius to maximum wind |
| | storm translation speed |
| | angle of approach |
| | maximum wind speed |
| | asymmetry |
| Topography | shelf width |
| | slope width |
| | slope of shelf |
| Model formulation | advection |
| | atmospheric pressure |
| | bottom friction |
| | external pressure |
| | internal pressure |
| | grid resolution |
| | entrainment formula |

extending 1000 km in the east-west direction, and 600 km in the north-south direction. Land was specified on the northern and southern boundaries. The latter was included for reasons which will be detailed in the section on boundary conditions.

Note that subsequent figures involving snapshots in time will be plotted in terms of $x$ position and/or $y$ position. The reader may always establish the absolute position by referencing Figure 1.

A north-south cross section of the basin is shown in Figure 2. It is characterized by a shelf width of 120 km and slope width of 80 km. These are mean values for the U.S. Gulf of Mexico shelf.

Response was monitored at the three sites indicated by triangles in Figures 1 and 2, and denoted as deep water, slope, and break, corresponding to the southern, central, and northern sites, respectively. The deepwater site was in the deepest part of the basin, 1000 m, and its response was found to be unaffected by topography in the upper three layers. The slope and break sites were located in 350 and 120 m of water, respectively. A shallower site was not possible because of the artificial step between 25 and 120 m. CT discuss the justification and need for this step.

The basin dimensions were selected to minimize the model domain (hence computer time) without introducing boundary influences other than from the shelf and coastline. Further runs were performed using a 20% larger north-south dimension, a 30% larger east-west dimension, and an abyssal water depth of 2000 m. The resulting responses at the three reference sites were found to vary by less than 3% from the base case.

### 2.2. Wind Field

A wind field closely approximating Hurricane Eloise from PR was used. Figure 3 shows a snapshot of the wind friction

velocity squared ($m^2 s^{-2}$) using the steady state wind field suggested by PR, and the drag law of *Garratt* [1977]. The wind field had peak winds of 32 m s$^{-1}$ and a radius to maximum winds of 40 km, and it was symmetrical.

The storm was initially started from the southern end of the basin as shown Figure 1. It was moved due north at 8.5 m s$^{-1}$, the speed used in PR's studies.

Note that the wind field extended only 300 km from the storm eye. This is in seeming disagreement with PR, who showed winds in excess of 10 m s$^{-1}$ extending 600 km from the storm eye. The region from 300 to 600 km was excluded to minimize the model domain and model run times. Neglect of this region had little effect on the response, as was proven by an additional run using a maximum extension of 400 km. This run showed a change of less than 1% from the response using 300 km.

### 2.3. Boundary Conditions

Initially, the basin was surrounded by land, in part because a land boundary is unambiguous and easily implemented in a numerical ocean model. However, boundary reflections due to external and internal inertio-gravity waves were quite energetic, and rapidly corrupted the model results. Thus it was necessary to specify a nonreflecting boundary condition. This requires novel techniques to handle internal and external modes simultaneously.

The flow relaxation scheme (FRS) is one method recently used successfully in a barotropic ocean model by *Martinsen and Engedahl* [1987] to simulate a nonreflecting boundary. The FRS was first used in multileveled atmospheric models by *Davies* [1973].

Briefly the scheme applies the expression

$$\Omega = \alpha \hat{\Omega} + (1 - \alpha)\tilde{\Omega} \qquad (1)$$

to each of the prognostic variables $\Omega$ (i.e., $u$, $v$, $h$, or $\rho$ for this model) in a boundary region, where a circumflex indicates that the variable is specified, a tilde indicates that the variable is calculated for the governing equations, and $\alpha$ is a specified relaxation parameter which varies from zero at the inner edge of the FRS region to one at the outer edge.

Implementation of the FRS scheme requires an additional boundary region on the edge of the grid. Further work documented by *Cooper* [1987] indicated that adequate damping was achieved when this region was nine elements wide. The choice is governed by the wavelength of the most energetic waves. Figure 1 includes this boundary region with its inner edge denoted by a dashed line.

The functional form of $\alpha$ must be empirically derived. Further work documented by *Cooper* [1987] suggested a relationship of the form

TABLE 2. Summary of Model Input Parameters for Default Case

| Latitude, °N | Initial Layer Thickness, m | Temperature, °C | Salinity | $c_b$, m s$^{-1}$ | Shelf Width, km | Slope Width, km | $\Delta r$, km |
| --- | --- | --- | --- | --- | --- | --- | --- |
| 24 | 30 | 28.75 | 36.30 | 0.001 | 120 | 80 | 20 |
| | 150 | 28.70 | 36.35 | | | | |
| | 250 | 14.70 | 36.90 | | | | |
| | 570 | 7.00 | 36.90 | | | | |
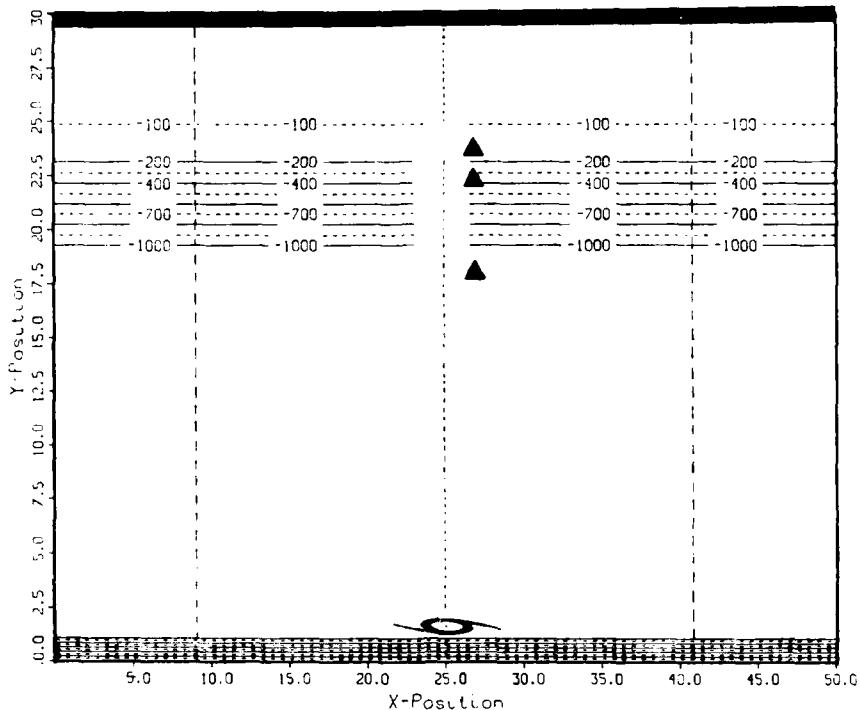
Fig. 1.  Model basin plan view. The figure shows the bathymetry of the model basin used in the sensitivity studies. The three triangles indicate the standard reference stations. The dashed lines indicate the outer edge of the active model domain and the inner edge of the boundary region. Results between the dashed line and outer boundary will not be realistic. The grid is composed of 20-km square elements.

$$\alpha = 1 - \tanh\left[(L - 1)/2\right] \tag{2}$$

for the western boundary, where $L$ is the grid counter in the east-west direction. A similar expression can be written for the eastern boundary.

To test the FRS scheme, the response was compared at three sites near the storm path for two grid systems: a full grid of the Gulf of Mexico and a subgrid of the gulf. Figure 4 shows the two grids. Both use the normal gulf topography described by CT. For the subgrid, an FRS region 10 elements wide was added to the east and west boundaries. Forcing was provided by the hurricane wind field described earlier, with the storm track depicted by the dotted line in the figure. The mixed-layer response was then monitored at the three reference sites indicated by the triangles in the figure.
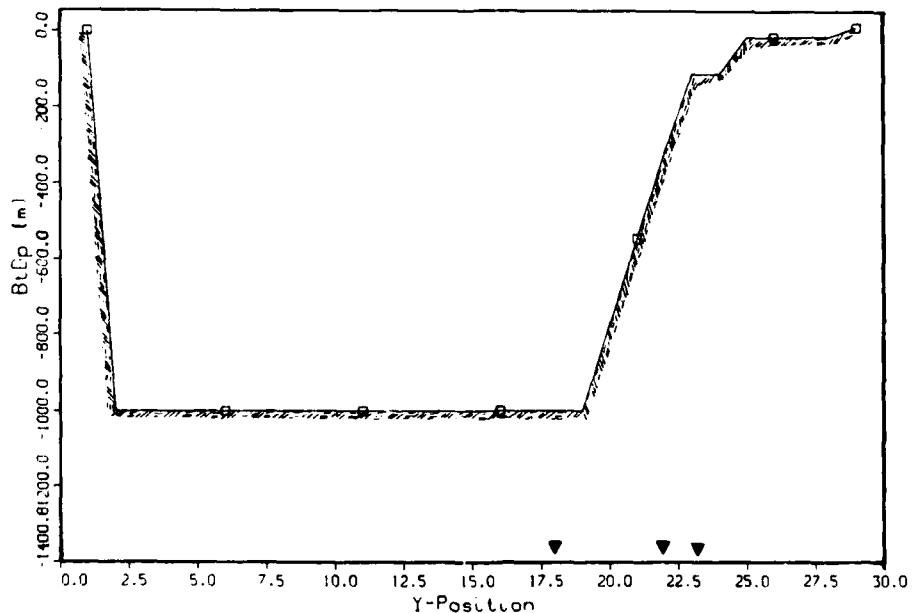


Fig. 2.  Model basin cross section. Figure shows cross section from the southern to northern boundaries. Each grid element is 0.2° square.
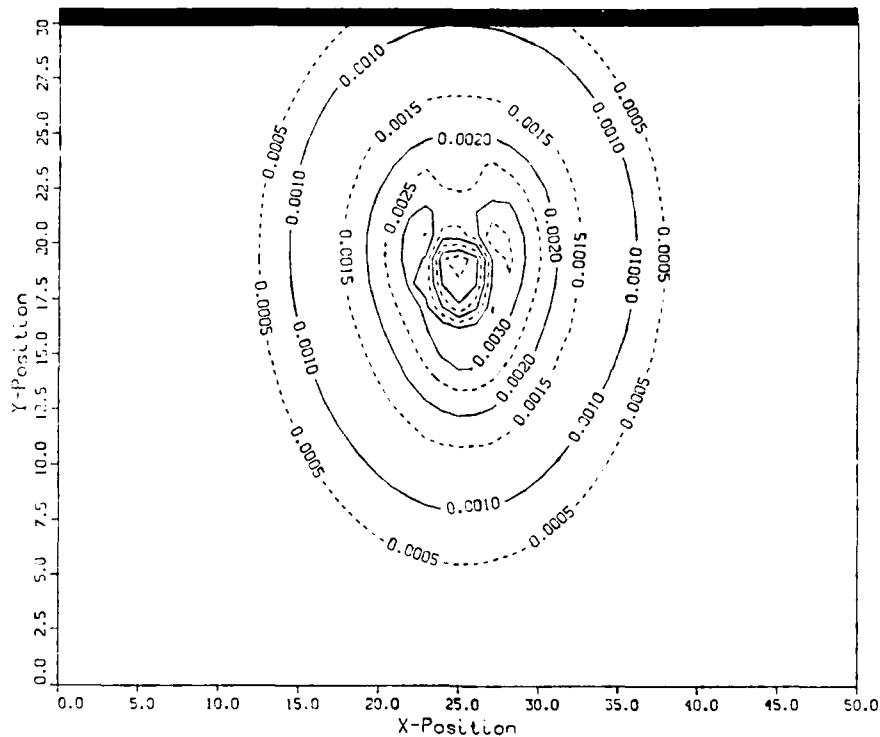
Fig. 3. Default wind field. The figure shows a snapshot of wind friction velocity squared ($m^2 s^{-2}$) contours. Wind field is based on model of Hurricane Eloise developed by *Price* [1981]. Each grid element is 20 km square.

Figure 5 shows a typical comparison for the intermediate or slope site. Following the first peak in the response at about 15 hours, discrepancies do start to appear, but these are relatively small. Most important, the two grids are essentially identical during the period of peak winds (13.3 hours), which is the period of interest to this study.

### 2.4. Results

*Free surface response.* Two features dominate the free surface field: a forced wave (storm surge) and an external wake. Both are visible in Figure 6, which shows a snapshot just as the storm passes onshore.
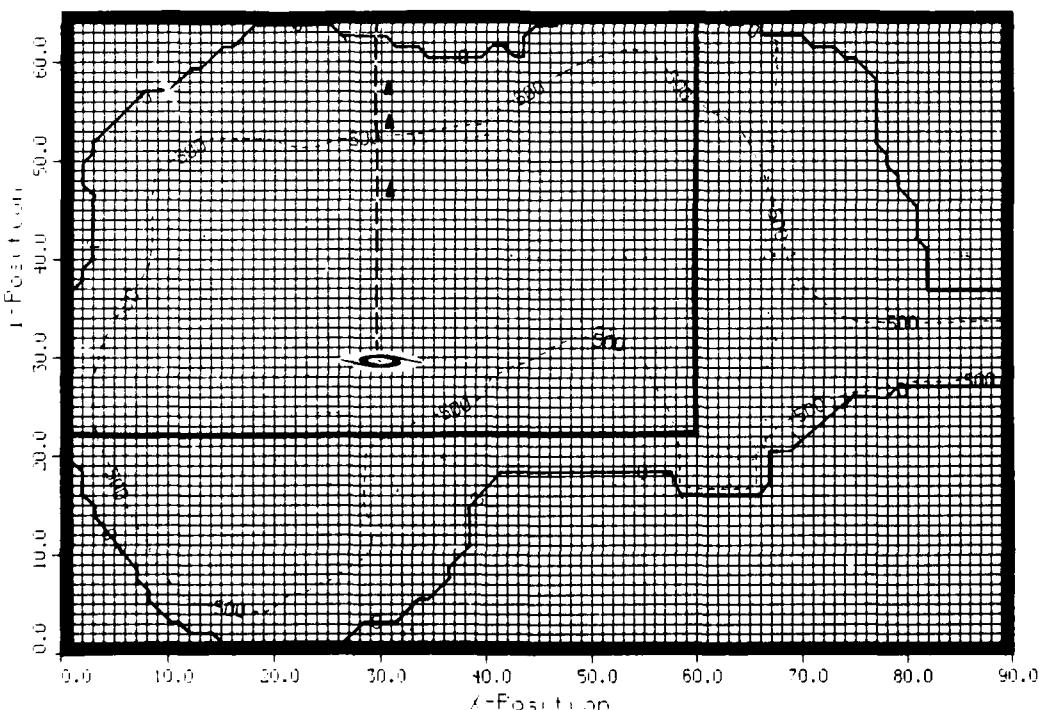


Fig. 4. Full and subgrid used for the three-dimensional test. The dark rectangular area denotes subgrid of 60 × 39 elements. Dotted line shows track of the storm center. Triangles show reference sites where comparisons between the two grid results are made. A grid element is 20 km square.
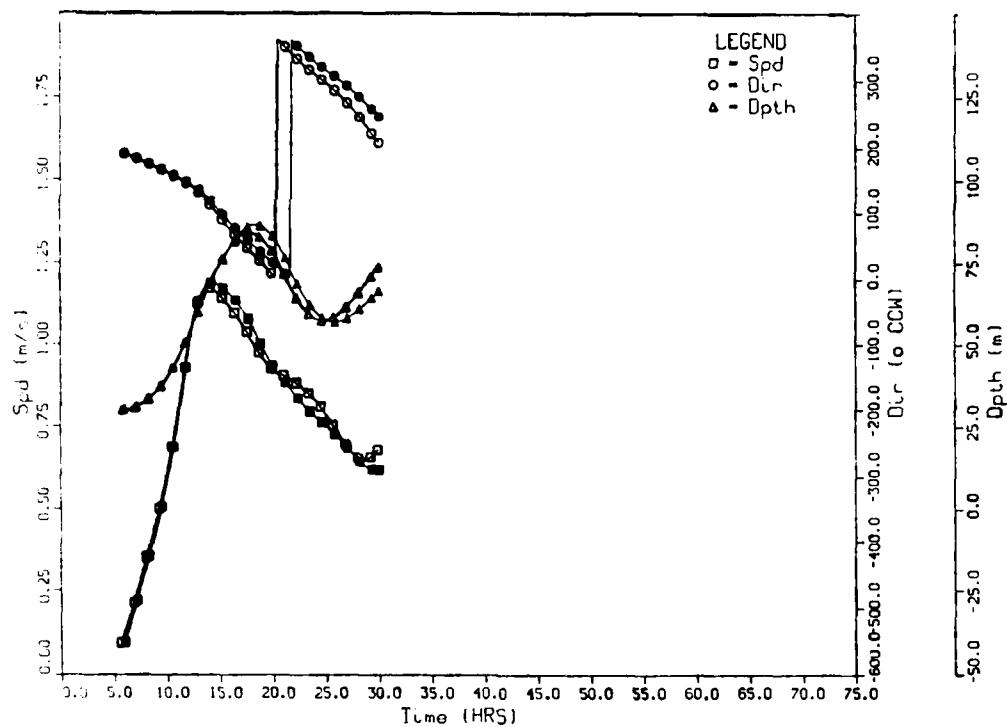
Fig. 5.   Comparison of response for subgrid (solid symbol) and full grid (open symbols). Figure shows the time series of mixed-layer speed, direction, and depth for the slope reference site. Peak winds occurred at 13.3 hours. Each grid element is 0.2° square.

The external wake appears in Figure 6 as the broad shallow trough centered at element (25,10). It has an inertial component of 0.05-m amplitude superimposed on a slowly relaxing mean depression of 0.15 m as depicted in the time series of surface elevation in Figure 7. This wake is due to baroclinic processes, as it does not appear in the single-layer model results.

The forced wave rapidly disappears as the storm goes onshore. It radiates free waves, some of which propagate as
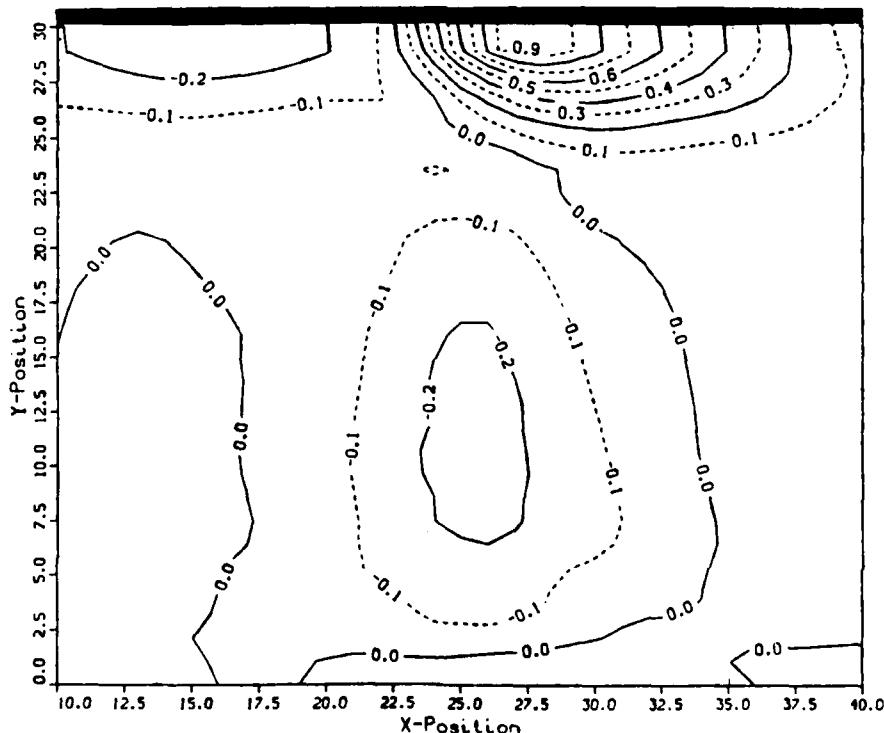


Fig. 6.   Storm surge and external wake. The figure shows free surface contours at 20 hours. Note the two dominant features: a forced wave (storm surge) along the coast, and an external wake indicated by the shallow trough of 0.2 m. The position of the storm is indicated by the storm symbol. Each grid element is 20 km square.
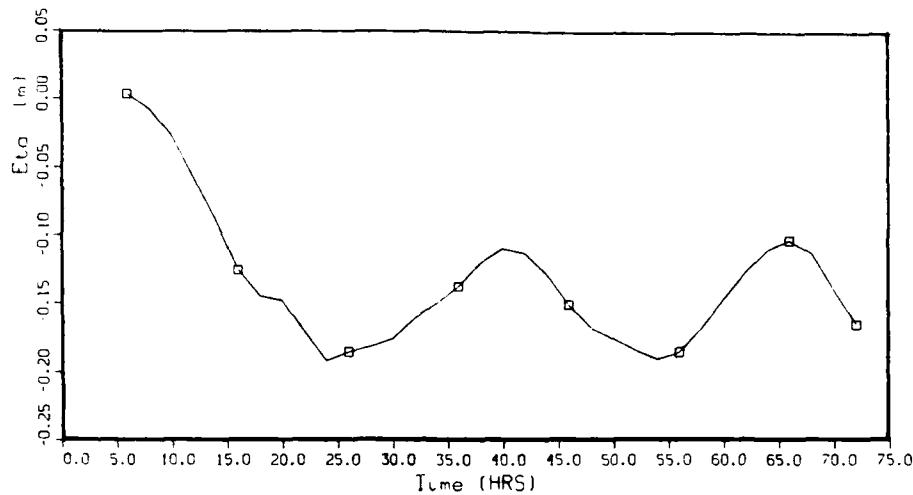
Fig. 7.  Time series of external wake. The figure shows a time series of surface elevation at the deepwater site. Note the inertial oscillation of 0.05-m amplitude superimposed on a slowly relaxing mean of 0.15 m.

edge waves to the west and east, and out of the basin. This behavior was documented by *Kuo and Ichiye* [1977].

At its peak, the forced wave extends from the shelf a distance of the same order as the wind field forcing. This is documented in Figure 8, which shows a cross-shelf section of the free surface elevation at the time the storm hits the coast. The exponential decay is apparent out to row 10, or roughly 280 km from the shelf break. This is comparable to the wind field shown in Figure 3.

*Velocity response.*   Figure 9 shows 6-hourly snapshots of the the mixed-layer velocity for one inertial period (30 hours) after the storm moves ashore. The response seaward of the break is strikingly similar to the deepwater response shown in Figure 10.

On the shelf, the response dampens rapidly. A transition zone becomes apparent between the shelf and deeper waters by about 24 hours. As discussed by CT, the transition zone is a consequence of the artificial step introduced into the model topography.

Comparisons of actual time series confirm that seaward of the break, the mixed-layer velocity response is essentially the deepwater response. This can be seen by comparing the cross-shelf velocities at the reference stations (Figure 11). The deepwater reference station shows no topographic effect, so it can be used as a point of comparison. The peak currents at the three sites agree to within a few percent.

During the poststorm period, the shelf influence is more substantial; note the increasing differences from the deepwater response at both the slope and break sites by the start of the second inertial period. The effect of topography on period and amplitude is variable. Amplitude is smaller at the slope site than at the break and deepwater sites. The period at the deepwater site is roughly 0.9 IP, while that of the slope site the period is slightly larger and that at the break site is slightly smaller.

The response in layer 3 shows that topography plays a larger role. It further suggests that the internal Rossby radius is the critical indicator of the shelf influence on the lower layer
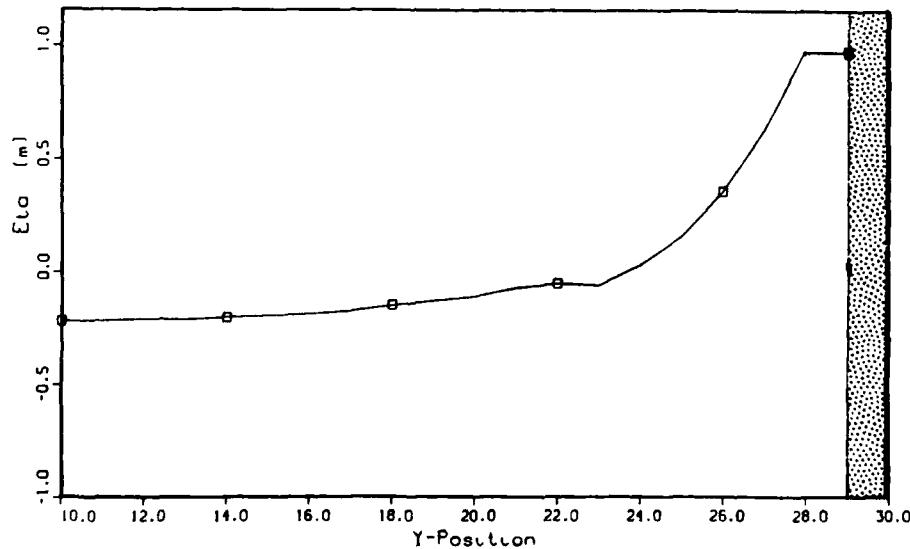


Fig. 8.   Shelf influence on free surface. The figure shows a snapshot of free surface along a cross-shelf section. The coast and shelf break are apparent at rows 20 and 23, respectively. The shelf influence is seen to extend to row 10 or 11. Each grid element is 20 km square.
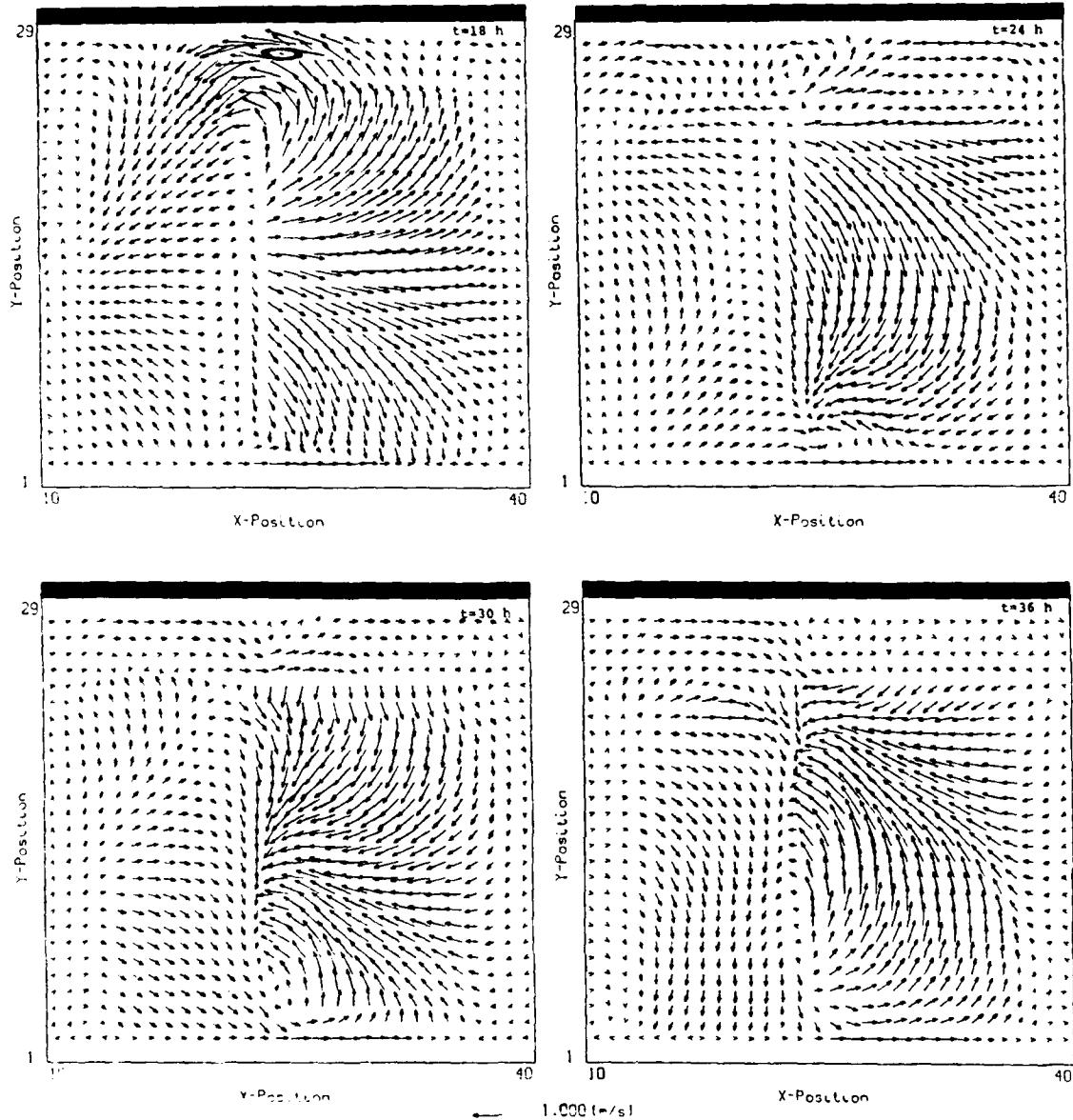
Fig. 9. Mixed-layer velocity response. The figure shows 6-hourly snapshots of the mixed-layer velocity. The
sequence covers one inertial period after the storm goes ashore. Each grid element is 20 km square.

velocity response. Figure 12 compares the cross-shelf velocity
at the deepwater and slope sites and at a site just seaward of the
slope site. The intermediate and deepwater sites are nearly
identical, while the slope site is much more energetic. Layer 3
at the slope site is 20 km away from land, or the same order as
the internal Rossby radius of deformation.

*Mixed-layer depth response.* A classical [*Geisler,* 1970]
deepwater wake dominates the mixed-layer depth response.
Figure 13 shows 6-hourly snapshots of the mixed-layer depth.
The snapshot at 18 hours is indistinguishable from a deepwater
response. Some topographic influence does appear in the next
snapshots in two forms: an alignment of the wake with the
shelf, and an increase in the amplitude of the wake. Both these
features appear in a region extending roughly 40 km from the
shelf break, or about one internal Rossby radius.

These observations are confirmed by comparing the time
series of mixed-layer depth at the three reference stations
(Figure 14). Note that the first maximum at the break site is
roughly 16% larger than the deepwater one. The influence of

the coast stops at the element just seaward of the slope site,
consistent with the Rossby radius scaling suggested from the
plan views. After 30 hours, the response at the slope site in
Figure 14 also suggests the presence of higher modes, and
perhaps some reflections.

*Momentum balances.* The momentum balance reveals
some dependence on water depth. Figure 15 displays the
time series of the various momentum terms in the mixed
layer at the three reference sites.

In deep water the balance is essentially inertial; all other
terms are nearly an order of magnitude less. As the water
depth decreases, the pressure gradient increases in impor-
tance, at times nearly rivaling the inertial balance. However,
pressure has little effect at the time of maximum winds.
Advection increases in importance in shallower water, al-
though it is always less than 20% of the total.

*Summary.* At the time of maximum winds the following
points are observed.

1.   The free surface response extends one external Rossby
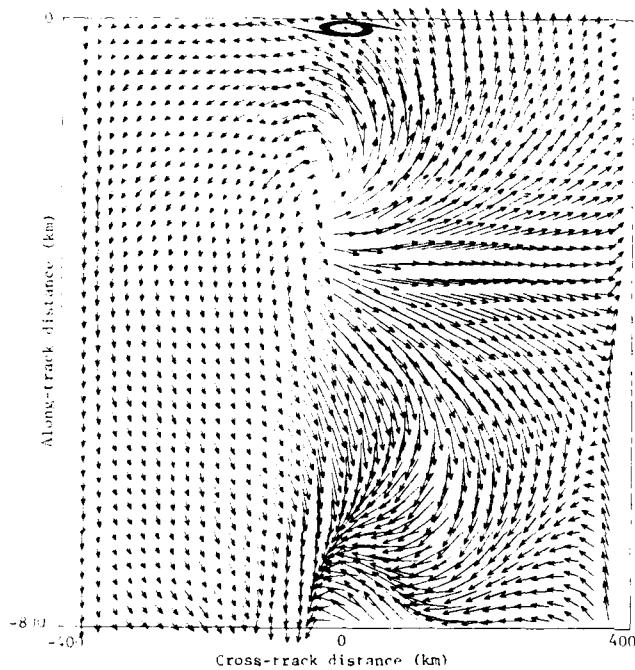
Fig. 10.    Quasi-steady solution of mixed-layer velocity vectors during Hurricane Eloise based on simulations from a Price-type model. Vectors are separated by 20 km. Maximum velocity vector shown is 110 cm s$^{-1}$. The location of the storm center is indicated by the storm symbol. The storm is moving from south to north at 8.5 m s$^{-1}$. Winds and initial conditions are same as those of PR.

radius from the shelf break. The forced wave generated by the storm dissipates into seaward radiating free waves and free edge waves. This occurs within 2 hours of storm landfall.

2.    The mixed-layer velocity response is strongly inertial, and there is only about a 10% difference observed between

mixed-layer velocities along a cross-slope section. Pressure gradients and advection do play a stronger role in shallower water, but their contribution is still small.

3.    Lower layer velocity response is more sensitive to topography. Lower thermocline velocities on the slope are triple those in deep water but are still small in magnitude (20 cm s$^{-1}$). Topographic effects extend to 20 km from the shelf (comparable to one internal Rossby radius).

4.    Mixed-layer depth increases slightly as water depth decreases. The difference between the deepwater and break sites is about 15%. Topographic influence extends one element from the shelf (comparable to one internal Rossby radius from the shelf).

After one inertial period of storm passage, the following points are observed.

1.    The free surface response is dominated by an external wake with cross-track horizontal length scale of the order of the storm, and a vertical magnitude characterized by an inertial oscillation of 0.05 m superimposed on a slowly relaxing depression of the order of 0.1 m.

2.    Mixed-layer velocities dampen much more quickly in shallower water; the e-folding scale was 3 times less for the break site than the deepwater site.

3.    Higher modes and/or reflections are apparent at the slope site.

3.    SENSITIVITY STUDY

3.1.    Background

A total of 14 parameters were studied, and these can be broken into three categories: storm parameters, topography, and model formulation. Table 1 summarizes the parameters.

Model results are summarized in Table 3. Within each category, the parameters are rank ordered according to their effect on the mixed-layer speed at the slope site.
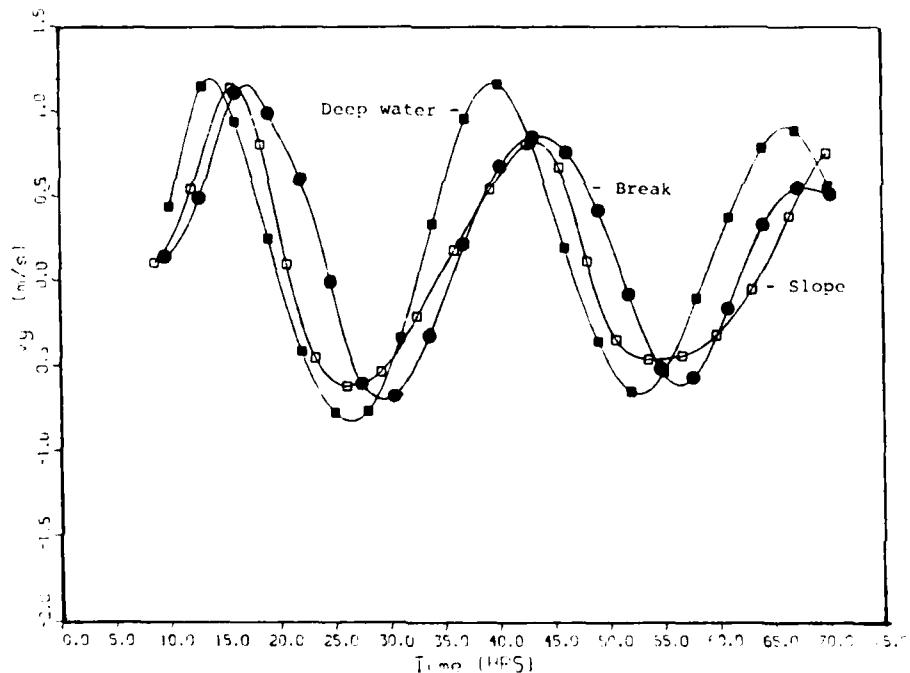


Fig. 11.    Shelf influence on mixed-layer velocities. The figure shows a time series of cross-shelf mixed-layer velocity at the three reference sites. Note that the time axis is not absolute time, but rather time relative to maximum winds at the particular site. Each grid element is 20 km square.
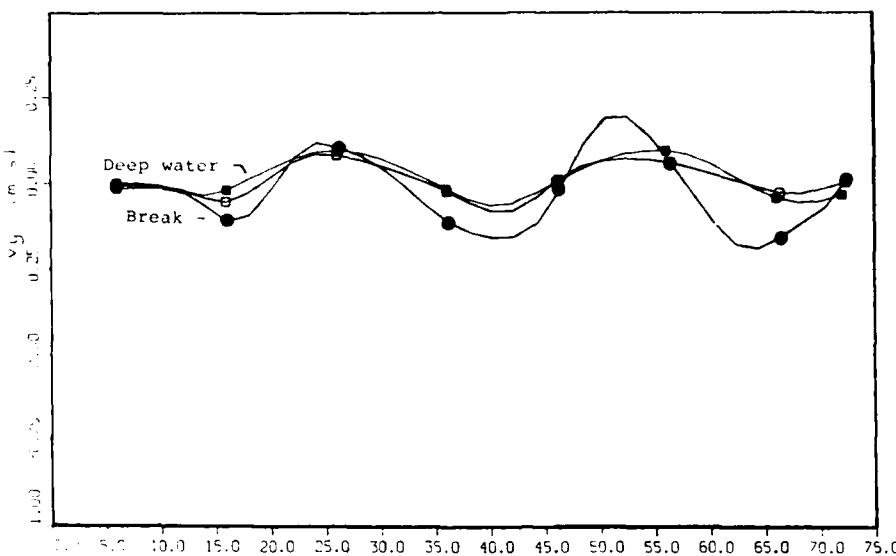
Fig. 12.    Shelf influence on lower layer velocities. The figure shows time series of cross-shelf velocities in the third layer at the deepwater and slope reference sites as well as the site just seaward of the slope site. Note that the time axis is not absolute time, but rather the time relative to maximum winds at the particular site.

At the top of the table the base-case response is given in terms of the mixed-layer speed (cm s$^{-1}$), compass heading (i.e., degrees relative to true north), and depth (in meters) at the time of peak winds. Response is shown for the three reference sites. Changes in the parameter are quantified in the column labeled Change. In many cases the parameter was simply switched on or off, and so this column is not applicable and is denoted by a blank.

In Table 3 the sensitivity cases are listed below the base case. For the sensitivity cases, the results are shown as the net change (percent) from the base case. That is, the response from a given case is subtracted from the base-case response, and the resultant is normalized by the base-case response and entered in the table. Values are shown to the nearest percent. A negative (positive) sign indicates there was a reduction (increase) in the response.

The decision to focus on the response at the time of maximum local winds was driven primarily by interest in the time period when peak loads on an offshore structure will be highest. This tends to occur when waves and winds are at their peak. Previous sensitivity studies of deepwater hurricane response [PR; Greatbatch, 1983, 1984] have focused on peak currents, which tend to occur several hours after peak winds. However, a review of the time series suggests that a shift of a few hours would make little difference in the results in Table 3.

### 3.2. Model Formulation

Barotropic and baroclinic response.    The baroclinic response dominates the barotropic response even at the relatively shallow break site. This is supported by two runs from a reduced gravity (RG) model which includes only the baroclinic response and a single-layer model which includes only the barotropic response (Table 3). It is apparent that the baroclinic response accounts for better than 90% of the speed at all three sites.

Interactions between baroclinic and barotropic modes and the effect of topography on the baroclinic response are apparent at the break site. This is documented in Figure 16, which compares the mixed-layer velocity at the time of peak winds from two different sources: the full model versus the resultant obtained by adding a purely barotropic result (one-layer model), and purely baroclinic result (RG model). The resultant overestimates the full model result by about 25%. At the slope site the difference between the full model and resultant differs by about 6%, suggesting that interactions are not important there.

The joint effect of baroclinicity and bottom relief (JEBAR [Huthnance, 1984]) may partially explain these results at the break site, despite the relatively short time scales involved [see Weaver and Hsieh, 1987]. However, the JEBAR effect does not seem to be significant at the slope site in these experiments. Additional experiments are needed to clarify the importance of JEBAR in generating the shelf wave response.

It should be noted that some of the 25% difference observed at the break site is no doubt due to the fact that the total wind energy input into the resultant is more than that input into the full model. Furthermore, even though the response does appear to be strongly baroclinic for this parameter space, it will be seen shortly that the angle of storm approach can accentuate the barotropic influence.

Entrainment formulation.    Results are sensitive to the entrainment formulation. This is supported by results in Table 3 which used the Kato and Phillips [1969] (henceforth referred to as KP) entrainment law rather than that of Pollard et al. [1983] (henceforth referred to as PRT). Changing to KP increases the mixed-layer velocity by roughly 15% above the PRT formulation. This increase is most pronounced at the slope site. Use of KP has less effect on mixed-layer depth. It decreases the depth in all cases, and the decrease is accentuated with depth.

The difference in the response obtained from the two formulations is much larger at the time of peak currents. For example, the velocity using KP is 37% larger than that using PRT at the slope site.
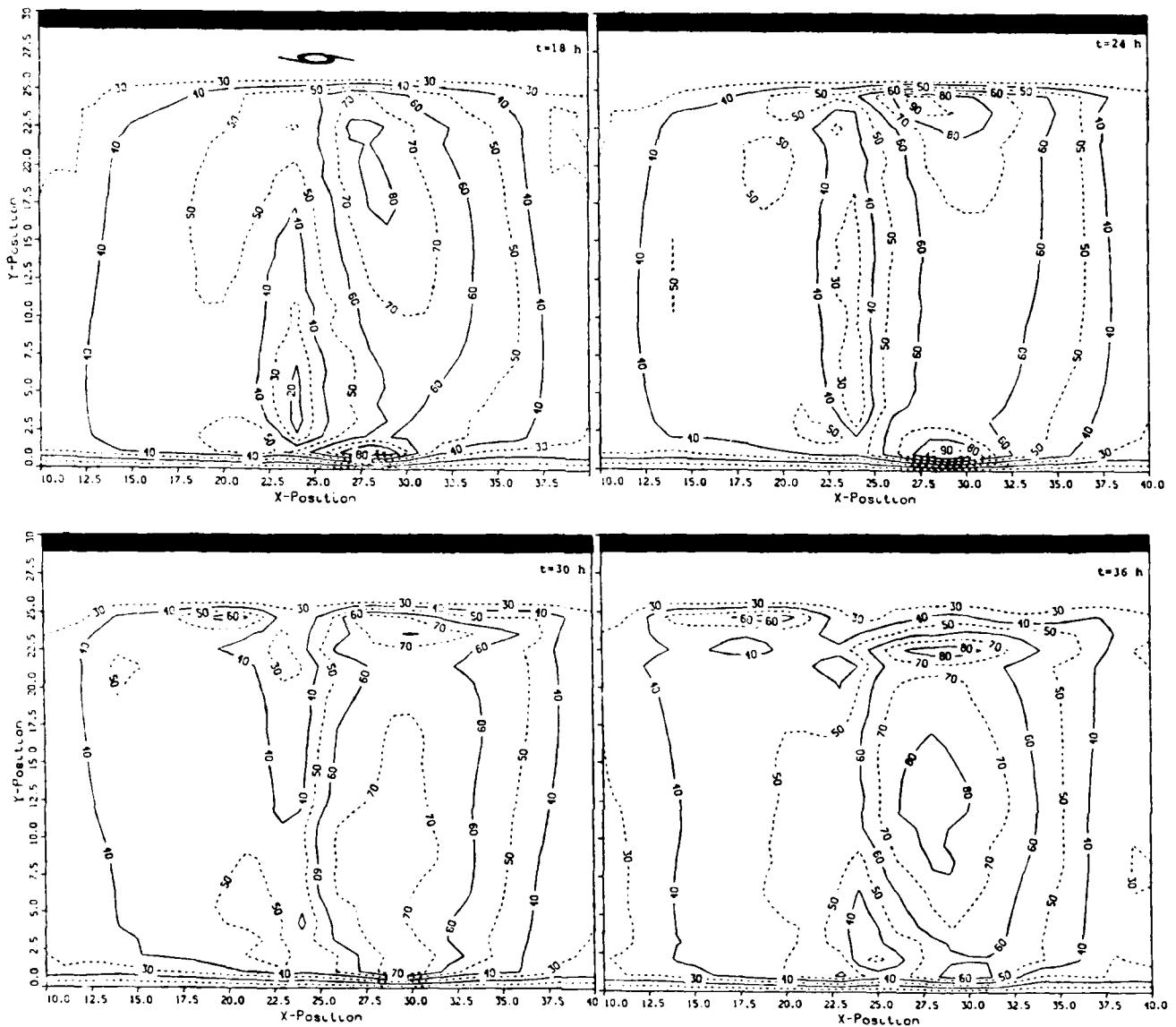
Fig. 13.    Mixed-layer depth response. The figure shows 6-hourly snapshots of the mixed-layer depth. The sequence covers one inertial period after the storm goes ashore. Each grid element is 20 km square.

*Advection.*    Advection is not important for fast moving storms but is important for slow ones. This is consistent with the findings of PR and *Greatbatch* [1983, 1984] and can be deduced from the information in Table 3. No advection for a fast moving storm corresponds to the default storm without advection. No advection for a slow moving storm corresponds to a storm moving at $\leq$ 25 m s$^{-1}$. The row labeled "translation speed" corresponds to the slow storm (4.25 m s$^{-1}$) with advection. The terms fast and slow are used because these qualitatively describe the translation relative to the mean of 6 m s$^{-1}$ in the Gulf of Mexico.

For the slow storm, advection substantially decreases the response. This is not as obvious from the table but can be inferred by comparing the slow moving storm values row with the translation speeds. This reveals that including advection reduces the velocity by roughly 15% and depth by 10% while increasing the direction by 5%. These represent mean values for the three sites. There the importance of advection is smallest at the shallow site, a fact which is probably explained by the larger barotropic contribution and

its relative insensitivity to advection. As noted by PR, the reason advection is important for the slow storm is because of increased Ekman pumping.

The importance of advection for the slow storm diminishes as the water depth decreases. This is because advection is more important for the baroclinic mode than for the barotropic modes. Since the baroclinic modes decrease in importance as water depth decreases, the importance of advection also decreases with water depth. For a purely barotropic response, advection is about 5% of the dominant term in the momentum balance, regardless of water depth, whereas for a purely baroclinic response, advection is about 25%.

*Pressure gradients.*    Pressure gradients are negligible in deep water but become somewhat more important as the water becomes shallower. This is evident from the results in Table 3. Model results for this case set the term $P = 0$ in the momentum equations. PR came to a similar conclusion regarding pressure gradients for his study.

The increase in importance of the pressure gradient with
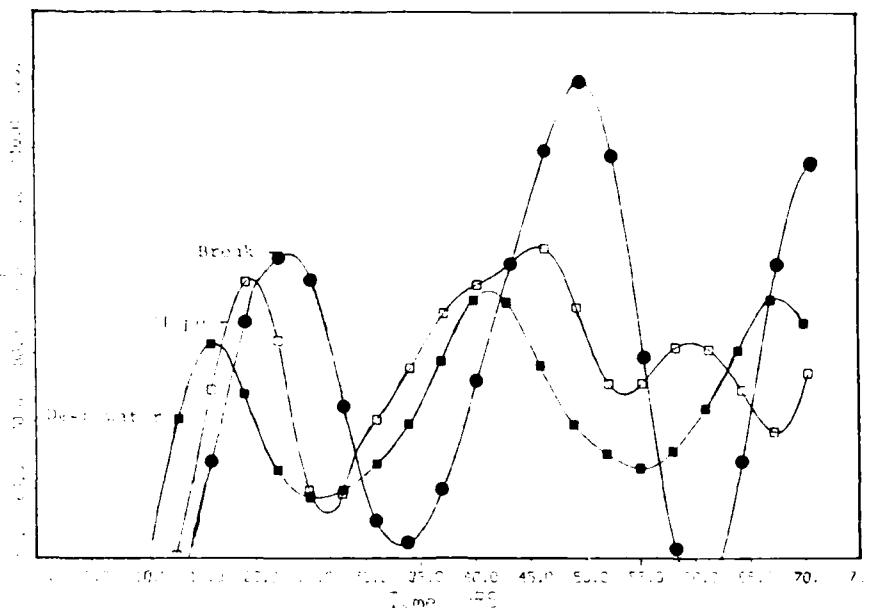
Fig. 14. Mixed-layer depth response. The figure shows a time series of mixed-layer depth at the three reference stations.

decrease in water depth is consistent with earlier observations that the barotropic mode plays a stronger role in shallower water.

*Grid resolution.* A 20-km grid is sufficient to resolve the mixed-layer response except perhaps near the break. This is deduced from $\Delta x$ in Table 3, which shows the change due to a reduction in the grid element size from 20 to 10 km.

### 3.3. Storm Parameters

*Wind speed.* Wind speed is one of the most important factors, as is indicated in Table 3. An increase in wind speed of 25% increases the water velocity by nearly 40%. Speed sensitivity is independent of depth and within 1% of that reported by PR for his deepwater case.

Depth response does intensify somewhat as the water depth decreases, and can be traced to the increasing contribution of the divergence terms in the continuity equation. This is deduced by comparing entrainment at the slope and break sites; entrainment is considerably larger at the slope site.

*Asymmetrical wind field.* An asymmetrical wind field was applied, and results are given in Table 3. Asymmetry was achieved by vector addition of one-half the storm translation speed (i.e., 4.25 m s$^{-1}$) to the local wind speed. This results in an increase in shear stress in the right half of the storm and a decrease in the left. The percentage increase or decrease is proportional to the distance from the eye. At the reference sites the winds increased by 13%.

The effect of asymmetry is to increase the response at the reference sites, but somewhat less than the sensitivity to wind speed alone would suggest. For example, at the break site the wind speed sensitivity results would suggest an increase of 20 and 15% for the speed and depth, respectively. However the actual increase is somewhat less for depth (14), and substantially less for speed (11).

*Storm approach.* The angle of approach of the storm has

an appreciable affect on the response. When the storm approaches at 45° to true north, the response is diminished, while a −45° approach accentuates the response (Table 3).

To understand this behavior, first note that most of the sensitivity is traced to the barotropic response. This is proven by reviewing equivalent runs using a one-layer model. These runs show that at the break site, a +45° approach reduces the response by 22 cm s$^{-1}$, while a −45° approach increased the response by 14 cm s$^{-1}$. These values compare nicely to the −26 and +12 cm s$^{-1}$ suggested from Table 3 for the full model runs.

The changes in response can be traced to the difference in the cross-shelf and alongshelf wind components. Figure 17 shows how the wind vector changes for the two cases at the break site. For the +45° case, the vectors have an initial on-shelf component. Therefore some of the input wind energy must generate a cross-shelf surface gradient to overcome the topographic gradient. However, for the −45° case, the wind vectors are initially more alongshelf and more readily generate alongshore motions.

This interpretation is supported by examining the cross-shelf momentum balance at the two sites (Figure 18). The reader should focus on near-peak velocities covering hours 10 to 25. For the +45° case the positive wind component results in a slow increase in velocity because of the opposing pressure gradient and inertia. Coriolis is only a slight factor. For the −45° case, Coriolis is substantial and reflects onshore Ekman transport. This transport creates a positive cross-shelf pressure gradient (negative pressure term), which in turn creates a geostrophic alongshelf current. Thus the response tends to be self-reinforcing

As indicated above, the +45° case will generate more potential energy during the storm approach, and this is apparent as a cross-shelf pressure gradient. The potential energy is transformed to kinetic energy once the storm passes. This is apparent in Figure 18 as a geostrophically balanced current flowing toward the east.
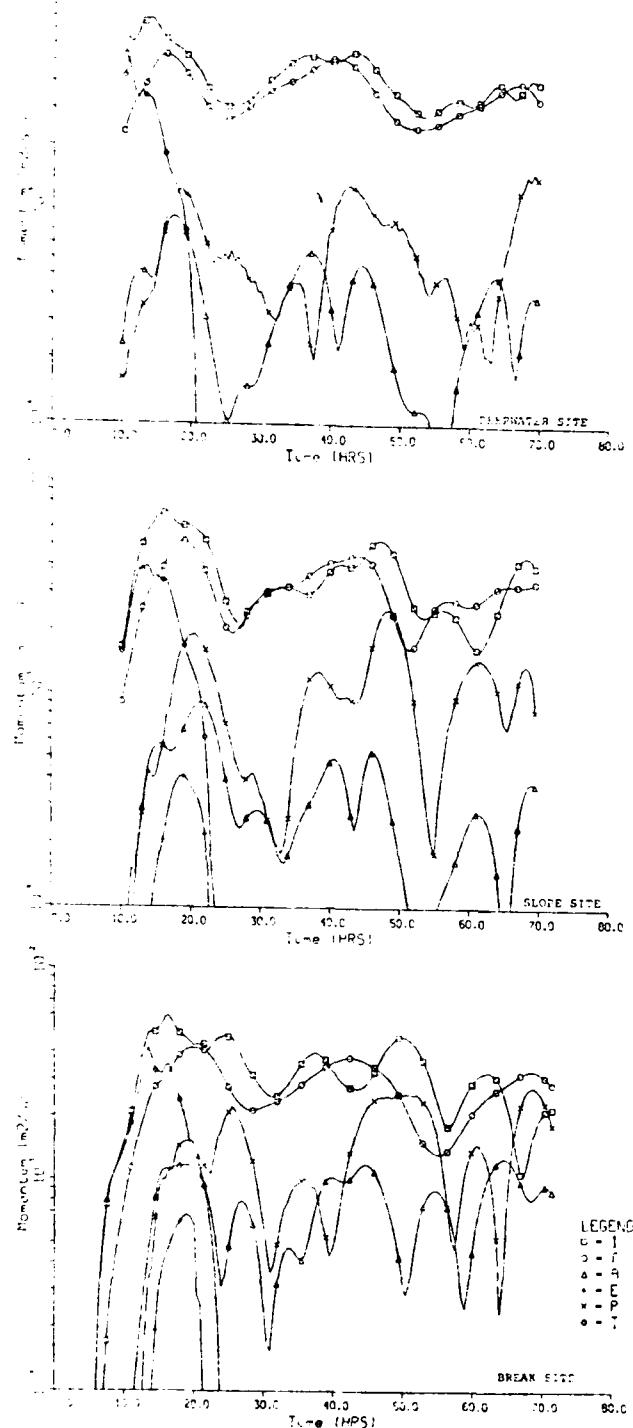
Fig. 15. Mixed-layer momentum balance. The figure shows a time series of mixed-layer momentum balance at the three reference sites where *I* is inertia, *f* is Coriolis, *A* is advection, *E* is entrainment, *P* is pressure gradient, and *T* is surface shear stress.

*Atmospheric pressure gradients.* Atmospheric pressure has a negligible influence in deep water and on the break and is only slightly apparent at the slope site. This is deduced from the $P_a$ values in Table 3. The weak response suggested in the results is consistent with *Kuo and Ichiye* [1977].

The results shown in the table use the radial atmospheric pressure distribution shown in Figure 19. It is derived from an average distribution of the Oceanweather winds while the eye was in the vicinity of EB-10. This is somewhat inconsistent, since the wind field used in the sensitivity study is from PR. Nevertheless, it was used for two reasons. First, PR did not suggest any pressure distribution; his wind field used actual observations. Second, the details of the pressure distribution are not critical in a sensitivity study.

*Storm translation speed.* Change in storm translation speed has a variable impact on the response. In the case of layer depth and direction, it is a major factor, but for velocities it is only minor. This is quantified by the translation speed values in Table 3. Results are based on a translation speed of 4.25 m s$^{-1}$, or one-half the default value of 8.5 m s$^{-1}$.

The enhanced response of the layer depth was documented by PR. It is due to an increase in Ekman pumping. That is, for the slower storm the Ekman response is larger. This causes a stronger divergence in the mixed layer just behind the storm center.

*Radius to maximum wind.* Changes in radius to maximum winds has some influence in deep water and at the break but is less important at the slope site. This is quantified by the radius values in Table 3, which used a radius of 20 k.n, or one-half the default value of 40 km.

The changes at the deepwater and break sites can be explained almost entirely by the 5% decrease in the local winds, which results from the decrease in radius. The wind sensitivity results suggest that a decrease of 5% in local winds should decrease the speed by 7% and the depth by 5%, and this compares reasonably well with the average decrease of 7% for speed and depth.

At the slope site the reduction is less than that anticipated from the wind speed sensitivity results. This is probably due to pressure gradients which alter the local balance.

### 3.4. Topography

*Shelf width.* Change in shelf width has a slight influence at the slope and break sites. This is documented by the shelf values (Table 3), which show results using a shelf of 160 km or one-third larger than the default value of 120 km. These small changes are consistent with the earlier observations that the response is primarily baroclinic. Thus topographic influences will extend relatively small distances of the order of 30 km, and so one would not expect to see results seaward of a site affected much by the topography to landward.

*Slope width.* Change in slope width has a negligible effect. This is quantified by the slope values (Table 3), which used a slope width of 160 km, or double the default value of 80 km. These findings are consistent with the results for shelf width.

*Artificial step.* The artificial step at 25–120 m does not affect the barotropic component seaward of the step. This is documented by the step values (Table 3), which show results for a one-layer model using a smooth bottom topography rather than the stepped topography of the default case. This conclusion is important in that it suggests that the step will not adversely influence the barotropic contribution at a site seaward of the step. A similar proof is not possible for the baroclinic contribution, but this is not of much concern, since the topographic influence will be limited to the internal Rossby radius, or only about 30 km.

TABLE 3. Summary of Model Sensitivities

| | Change, % | Deep Water | | | Slope | | | Break | | |
|---|---|---|---|---|---|---|---|---|---|---|
| | | Speed | Direction | Hour | Speed | Direction | Hour | Speed | Direction | Hour |
| *Default* | | | | | | | | | | |
| | 0 | 100 | 300 | 60 | 105 | 330 | 60 | 115 | 327 | 58 |
| *Model* | | | | | | | | | | |
| Barotropic | | -95 | -2 | | -87 | -2 | | -65 | -2 | |
| KP entrainment | | 10 | 0 | -3 | 21 | 0 | -10 | 15 | 0 | -10 |
| No advection slow moving storm | | 17 | 7 | 38 | 14 | 7 | 47 | 7 | 2 | 34 |
| Pressure | | 3 | 0 | 0 | 12 | 0 | 0 | 10 | 0 | -2 |
| Baroclinic | | 0 | 0 | 0 | 8 | 2 | 0 | -1 | 2 | 9 |
| $\Delta x$ | -50 | 0 | 0 | 0 | 0 | 0 | 0 | 7 | 0 | 0 |
| No advection, fast moving storm | | 0 | 0 | 0 | 0 | 0 | 0 | 0 | 0 | 0 |
| Friction | 100 | 0 | 0 | 0 | 0 | 0 | 0 | 0 | 0 | 0 |
| *Storm* | | | | | | | | | | |
| Wind speed | +25 | 38 | 0 | 21 | 39 | 0 | 23 | 38 | 0 | 28 |
| Asymmetrical | | 12 | 0 | 3 | 16 | 0 | 7 | 11 | 0 | 14 |
| Negative angle | -13 | 0 | 14 | 0 | 14 | -8 | 12 | 10 | -7 | 7 |
| Positive angle | +13 | 0 | 14 | 0 | -11 | 7 | -2 | -23 | 9 | -14 |
| $P_a$ | | 0 | 0 | 0 | 5 | 0 | 1 | 0 | 0 | 0 |
| Translation speed | -50 | 0 | 9 | 28 | -3 | 12 | 50 | -7 | 7 | 43 |
| Radius | -50 | -7 | 0 | -7 | -2 | 0 | -1 | -7 | 0 | -7 |
| *Topography* | | | | | | | | | | |
| Shelf | 100 | 0 | 0 | 0 | 2 | -3 | 0 | -6 | 0 | -7 |
| Slope | 100 | 0 | 0 | 0 | 0 | 0 | 0 | -2 | 0 | 0 |
| Step | | 0 | 0 | 0 | 0 | 0 | 0 | 0 | 0 | 0 |

Blanks indicate that parameter is not applicable. Units for the first row are centimeters per second for speed and degrees (heading) for direction. All subsequent rows are in percentages of the first row.

## 4. SUMMARY

A numerical model described and verified in part 1 of this two-part series [*Cooper and Thompson*, this issue] is applied to study the sensitivity of hurricane-generated currents on the outer shelf and slope. Numerical experiments were performed in a simple basin with a straight shelf. The sensitivity of the response to changes in storm parameters, direction of storm approach, and topography was quantified.

Reviewing these results gives considerable insight into the important processes affecting the ocean's response on the outer shelf and allows us to answer, in part, the questions posed in the introduction. Since these sensitivity studies have focused only on the mixed-layer velocity and depth at the time of peak winds, it can be argued that the sensitivity elsewhere in time and space may exhibit a different behavior. However, the present choice of response parameters
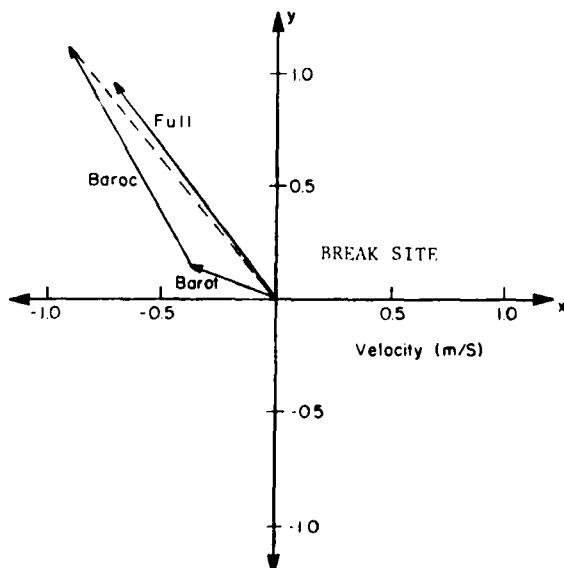
Fig. 16. Nonlinear interaction and topography effects. The figure shows the mixed-layer velocity vector at the time of maximum winds from three models: one layer, RG, and four layers corresponding to the barotropic, baroclinic, and full response, respectively. The dashed line shows the resultant obtained by superimposing baroclinic and barotropic responses. Results are taken at the break site.
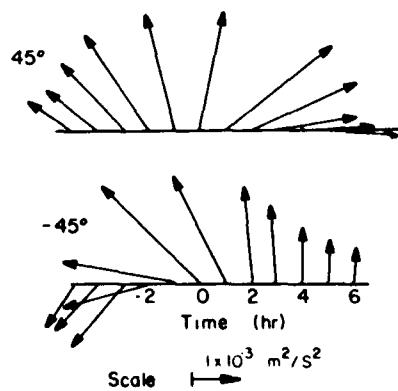
Fig. 17. Effect of storm approach on local wind stress at break site. The figure shows time series of wind stress vectors for storm with two approaches. A vector pointing straight up indicates wind blowing toward north. The top panel shows the storm translating toward northeast (+45°), while the bottom panel shows the storm translating toward northwest (-45°).
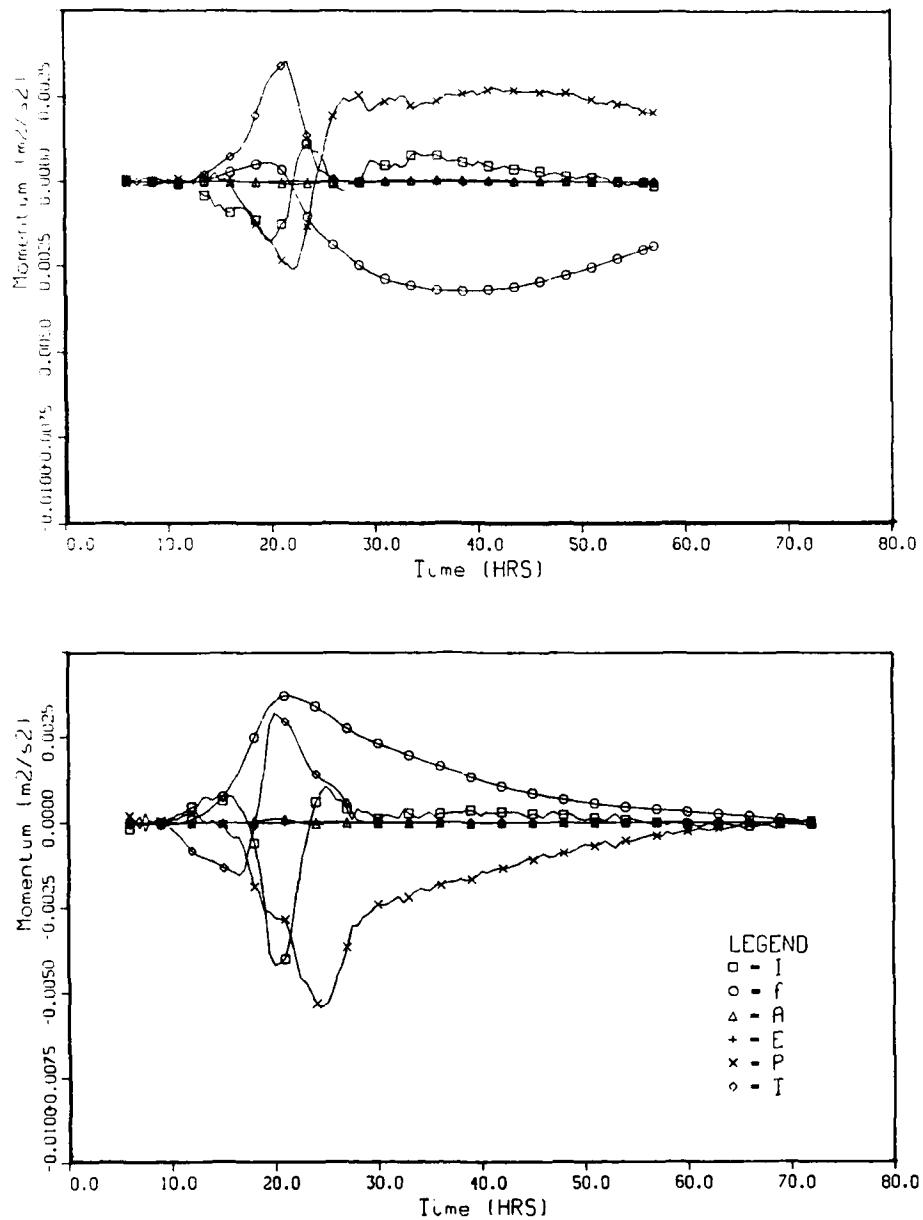
Fig. 18.   Effect of storm approach on cross-shelf momentum balance. The figure shows a time series of cross-shelf momentum terms at break site, where abbreviations are the same as in Figure 15. The top panel shows storm translating toward northeast (+45°), while the bottom panel shows storm translating toward northwest (−45°).

does reflect the sensitivity of the currents in the lower layers and the maximum current in the storm. The first follows because of the strong coupling between mixed-layer and sublayer responses. The latter follows because of the high correlation observed between currents at peak winds and maximum currents.

### 4.1.   Horizontal Gradient Terms

What is the relative importance of the horizontal gradient terms?

As suggested by PR and others, advection is negligible except for slow moving storms (less than 6 m s$^{-1}$). This is true for all three sites. For slow moving storms the importance of advection decreases slightly as the water depth decreases. This is due to the increasing importance of the barotropic component in shallow water, a component which is relatively insensitive to advection.
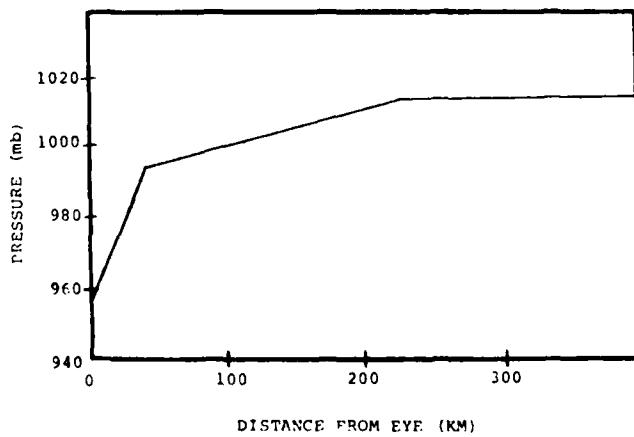


Fig. 19.   Radial atmospheric pressure distribution used in the sensitivity study.

Internal pressure gradients are negligible in deep water, a conclusion reached by PR and strongly implied by the success of one-dimensional models in predicting response [e.g., Martin, 1982]. However, as one moves onto the shelf, the importance of horizontal gradients increases. The gradients increase the speed by roughly 10% at the slope and break sites. This increase can be traced to the barotropic pressure field.

### 4.2. Response to Storm

How does the response depend upon translation speed, size, intensity, and angle of approach of the hurricane?

Changes in translation speed have a variable impact on the response. The mixed-layer velocity is fairly insensitive to variations (less than 8%), while direction and depth are quite sensitive. This behavior was noted by PR and is attributable primarily to the strong entrainment which occurs during the slower moving storms. The sensitivity is most pronounced at the slope site.

Change in storm size as measured by the radius to maximum winds has little influence. Observed changes can be largely explained by the change in local wind stress.

Storm intensity as measured by the maximum wind speed is a major factor in determining the response. Its influence is independent of water depth.

The angle of approach of the storm to the shelf is moderately important in shallower water. Both the slope and break sites experience changes of order 10%. When the storm approaches at a negative angle (i.e., storm moving to the northwest), the response is enhanced; when it approaches at a positive angle, the response is diminished. This is a reflection of the barotropic response. In the case of the negative angle, the time history of the wind stress vectors before the storm tends to be alongshelf. This causes a rise in sea level to balance the resistance to the resulting on-shelf Ekman transport. This forced wave provides a pressure gradient which augments the local winds at the time of peak winds.

### 4.3. Nonlinear Interaction

Is there substantial nonlinear interaction between modes?

The model results suggest that the interaction between barotropic and baroclinic modes is apparent only at the break, where it is relatively small (about 10%).

### 4.4. Cross-Shelf Dimensions

How is the response affected by the cross-shelf dimensions of the shelf and slope?

Cross-shelf dimensions of the slope have a negligible effect on the response. However, the dimensions of the shelf do have a moderate influence at the break.

### 4.5. Transition

Where does transition occur between primarily shallow shelf (barotropic) and primarily deep ocean (baroclinic)?

The response in this model is primarily baroclinic. Even in water as shallow as 120 m (break site), the baroclinic component contributes roughly 65% of the mixed-layer velocity signal. This can be reduced somewhat if the storm approaches at acute angles to the coast, but the baroclinic signal remains the dominant component.

Although revealing, this research leaves a number of unanswered questions. Two have already been mentioned in part 1: the interaction of the hurricane response with non-storm currents such as warm-core rings, and the nature of the response in water depths from 40 to 100 m. A third, alluded to earlier, concerns the unresolved contribution of JEBAR in generating the shelf wave response.

### REFERENCES

Cooper, C. K., Hurricane-generated currents on the outer continental shelf. Ph.D. thesis, 183 pp., Univ. of Maine, Orono, 1987.

Cooper, C. K., and J. D. Thompson, Hurricane-generated currents on the outer continental shelf, 1, Model formulation and verification, J. Geophys. Res., this issue.

Davies, H. C., A lateral boundary formulation for multi-level prediction models, Q. J. R. Meteorol. Soc., 102, 405–418, 1973.

Garratt, J. R., Review of drag coefficients over oceans and continents, Mon. Weather Rev., 105, 915–929, 1977.

Geisler, J. E., Linear theory of the response of a two-layer ocean to a moving hurricane, Geophys. Fluid Dyn., 1, 249–272, 1970.

Greatbatch, R. J., On the response of the ocean to a moving storm: The nonlinear dynamics, J. Phys. Oceanogr., 13, 357–367, 1983.

Greatbatch, R. J., On the response of the ocean to a moving storm: Parameters and scales, J. Phys. Oceanogr., 14, 59–78, 1984.

Huthnance, J. M., Slope currents and "JEBAR," J. Phys. Oceanogr., 14, 795–810, 1984.

Kato, H., and O. M. Phillips, On the penetration of a turbulent layer into stratified fluid, J. Fluid Mech., 7, 643–655, 1969.

Kuo, H., and T. Ichiye, A numerical study of the response of a barotropic ocean to a moving hurricane, Tellus, 29, 560–571, 1977.

Martin, P. J., Mixed-layer simulation of buoy observations taken during Hurricane Eloise, J. Geophys. Res., 87, 409–427, 1982.

Pollard, R. T., P. B. Rhines, and R. O. R. Y. Thompson, The deepening of the wind-mixed layer, Geophys. Fluid Dyn., 3, 381–404, 1983.

Price, J. F., Upper ocean response to a hurricane, J. Phys. Oceanogr., 11, 153–175, 1981.

Weaver, A. J., and W. W. Hsieh, The influence of buoyancy flux from estuaries on continental shelf circulation, J. Phys. Oceanogr., 17, 2127–2140, 1987.

C. Cooper, Coastal Leasing, 127 Sidney Street, Cambridge, MA 02139.

J. D. Thompson, Ocean Sensing and Prediction Division, Naval Ocean Research and Development Activity, Stennis Space Center, MS 39529.